

## Deliquescence and efflorescence of small particles

Robert McGraw<sup>a)</sup> and Ernie R. Lewis

*Department of Environmental Sciences, Atmospheric Sciences Division, Brookhaven National Laboratory, Upton, New York 11973, USA*

(Received 10 June 2009; accepted 28 September 2009; published online 20 November 2009)

We examine size-dependent deliquescence/efflorescence phase transformation for particles down to several nanometers in size. Thermodynamic properties of inorganic salt particles, coated with aqueous solution layers of varying thickness and surrounded by vapor, are analyzed. A thin layer criterion (TLC) is introduced to define a limiting deliquescence relative humidity ( $RH_D$ ) for small particles. This requires: (1) equality of chemical potentials between salt in an undissolved core, and thin adsorbed solution layer, and (2) equality of chemical potentials between water in the thin layer and vapor phase. The usual bulk deliquescence conditions are recovered in the limit of large dry particle size. Nanosize particles are found to deliquesce at relative humidity just below the  $RH_D$  on crossing a nucleation barrier, located at a critical solution layer thickness. This barrier vanishes precisely at the  $RH_D$  defined by the TLC. Concepts and methods from nucleation theory including the kinetic potential, self-consistent nucleation theory, nucleation theorems, and the Gibbs dividing surface provide theoretical foundation and point to unifying features of small particle deliquescence/efflorescence processes. These include common thermodynamic area constructions, useful for interpretation of small particle water uptake measurements, and a common free-energy surface, with constant RH cross sections describing deliquescence and efflorescence related through the nucleation theorem. © 2009 American Institute of Physics. [doi:10.1063/1.3251056]

### I. INTRODUCTION

Following uptake of water by deliquescence, atmospheric particles can easily grow to several times their dry diameter. The larger particles are more efficient scatterers of visible light, condensation sinks for condensable vapors, and sites onto which cloud droplets can form. Heterogeneous chemical transformations are also affected by the water uptake. For example, sulfate formation in aqueous particles proceeds through the partitioning of  $SO_2$  to the aqueous phase followed by aqueous-phase oxidation to sulfate whereas efflorescence to a crystalline particle removes this pathway. Through such effects, hygroscopic particle growth has important consequences for aerosol radiative forcing of climate both directly, through short-wavelength scattering, and indirectly, through cloud modification.

Particles respond to changes in relative humidity differently depending on their size and composition.<sup>1</sup> The present study examines particles that undergo deliquescent and efflorescent phase transitions with cycles of relative humidity (e.g., many inorganic salts) but the methods introduced, in particular the application of kinetic potential theory from nucleation (Appendix), should be applicable to general problems involving evaporation and condensation kinetics.

Early laboratory measurements of particle phase transformations focused on micron-size levitated particles.<sup>2-4</sup> These measurements produced valuable thermodynamic information on the densities and water activities of metastable supersaturated drops under bulk conditions; the levitated droplets being too large to have appreciable surface

effects.<sup>2,4</sup> In recent years, tandem differential mobility analyzers have been used to measure properties down to just a few nanometers in particle diameter, which is well into the realm of surface free energy influence and associated small particle effects.<sup>5-8</sup> The present study is aimed at understanding these small-particle phase transformations and their connection to bulk behavior.

Several theoretical studies over the past decade focused on particle size effects during deliquescence,<sup>9-11</sup> and on the nucleation of efflorescence.<sup>12,13</sup> In the bulk limit where the theory is well established, deliquescence is known to occur sharply with increasing relative humidity on reaching free energy equality between the initial (salt particle plus vapor) and final (fully dissolved solution drop plus vapor) states.<sup>14</sup> Equivalently, bulk deliquescence occurs under conditions that (1) the chemical potential of salt in the final solution equals the chemical potential of salt in the (pretransition) bulk crystal and (2) the chemical potential of water in solution equals that of the vapor. The first condition assures a saturated solution while the second gives a deliquescence relative humidity ( $RH_D$ ) equal to the RH over the saturated solution. For small systems the theories tend to diverge, as do the criteria for predicting deliquescence RH, which can differ significantly from the bulk. Several authors retain the criterion of free-energy equality<sup>9,11</sup> into the nanoregime while Djikaev *et al.*<sup>10</sup> demonstrate the existence of a nucleationlike barrier to the deliquescence of small particles that can effectively prevent the process until conditions are such that the barrier vanishes. The latter situation is reminiscent of the transformation of atmospheric aerosols particles to form cloud droplets as described by the Köhler theory.<sup>15</sup> There appears to be no general agreement as to which criterion to

<sup>a)</sup>Electronic mail: rlm@bnl.gov.

use and subsequent authors either extended free energy equality<sup>7</sup> or applied the vanishing barrier criterion<sup>16</sup> to predict deliquescence in the small particle regime.

The present analysis supports the vanishing barrier criterion. This is reformulated in Sec. IV to preserve the idea of chemical potential equality, as in the bulk limit, but applied to a predeliquescence state consisting of a salt particle core surrounded by a thin layer of solution. This physical picture is consistent with studies indicating that salt surfaces are thinly coated with water even at RH values far below the deliquescence point.<sup>17</sup> We find barrierless deliquescence initiated under the (unstable) equilibrium conditions that (1) the chemical potential of salt in the core equals that in the thin solution layer and (2) the chemical potential of water in the solution layer equals that of the vapor. These are clear generalizations to arbitrary size of the corresponding bulk criteria given above, but only in the bulk limit is this thin layer criteria (TLC) equivalent to free energy equality. We will show that for very small particles (ca. 1 nm radius) deliquescence can occur through a barrier crossing (nucleation) mechanism at relative humidities well below the  $RH_D$  predicted by the TLC. But for sodium chloride particles in the smallest size range of available measurements (5–10 nm diameter) the lowering of relative humidity relative to the TLC activationless limit, enabled by the nucleation mechanism, is about 1%–2%, roughly comparable to and thus indistinguishable from uncertainty in RH measurement. Thus the TLC should be a useful predictor of deliquescence except at the smallest particle sizes, below which deliquescence becomes a nucleation phenomenon that can be predicted using methods from nucleation theory as described below.

Thermodynamic properties of the coated particles are developed for layers of any thickness in Sec. II. Analysis is carried out here first using the classical capillary drop model, and then extended using the more complete Gibbs dividing surface model to obtain a self-consistent theory for small particles that includes interfacial tension composition dependence. Section III develops Maxwell-like area constructions that provide useful geometric interpretations for chemical potential and free-energy differences and facilitate the calculation of these quantities directly from measurement. For small droplets our results lead to a unified treatment of the deliquescence and efflorescence processes with connections to the Köhler theory and nucleation. The most significant results lie in the natural extension of methods from nucleation theory, specifically self-consistent nucleation theory,<sup>18</sup> kinetic potential theory,<sup>19</sup> and nucleation theorems<sup>20,21</sup> to deliquescence and efflorescence processes. Binary (salt-water) free energy surfaces for deliquescence and efflorescence at different relative humidities are shown to be connected through a simple linear relationship in particle water content that is closely related to the nucleation theorem. Nucleation barrier heights for deliquescence, efflorescence, and the overall change in free energy associated with deliquescence are obtained graphically through the area constructions derived from coexistence curves for solution drops and mixed-phase particles in equilibrium (stable or unstable) with vapor. Changes in barrier height with RH are obtained using nucleation theorems similar to those previously devel-

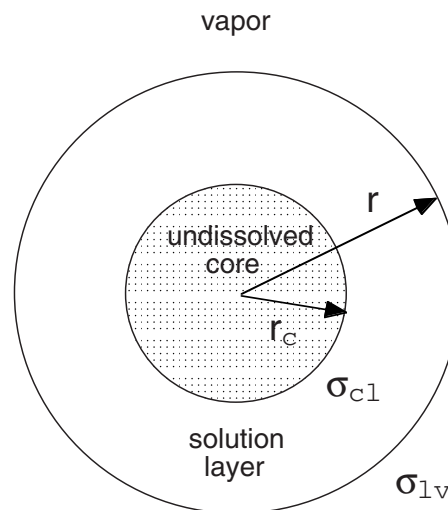


FIG. 1. Mixed-phase particle indicating overall particle radius  $r$ , radius of the undissolved core,  $r_c$ , and interfacial tensions of the core-solution and solution-vapor interfaces,  $\sigma_{cl}$  and  $\sigma_{lv}$ , respectively.

oped for binary vapor-liquid nucleation but applied here to deliquescence and efflorescence. The investigation of these unifying similarities between deliquescence and efflorescence and exploitation of their connections to nucleation theory are the focus of the present study.

## II. THERMODYNAMICS OF THE LAYERED PARTICLE IN THE CLASSICAL LIQUID DROP AND GIBBS DIVIDING SURFACE MODELS

Consider a mixed-phase drop of radius  $r$  inside of which is a spherical core of undissolved nonvolatile salt of radius  $r_c$  (Fig. 1). The drop together with its surrounding vapor is treated as a closed system with fixed total amounts of water and salt at constant temperature and pressure. Thus the system is free to exchange heat and volume work with its environment but not mass. For water there are  $N$  molecules total in the system split between  $n_1$  molecules in the solution and  $N - n_1$  in the vapor. Similarly there are  $n_{dry}$  salt molecules in the system split between  $n_2$  in the solution and  $n_{dry} - n_2$  in the undissolved core. The Gibbs free energy for the system is<sup>11</sup>

$$G_A = (N - n_1)\mu_1^v + n_1\bar{\mu}_1^{\text{sol}} + n_2\bar{\mu}_2^{\text{sol}} + (n_{dry} - n_2)\bar{\mu}_2^c + \sigma_{cl}A_c + \sigma_{lv}A, \quad (2.1a)$$

where  $\mu_1^v$  and  $\bar{\mu}_1^{\text{sol}}$  are the chemical potentials for water in the vapor and in solution and  $\bar{\mu}_2^{\text{sol}}$  and  $\bar{\mu}_2^c$  are the chemical potentials for salt in solution and in the undissolved core.  $\sigma_{cl}$  and  $\sigma_{lv}$  are the surface tensions of the core-liquid and liquid-vapor interfaces, respectively, and  $A_c$  and  $A$  are the corresponding surface areas. Equation (2.1a) gives the free energy of the layered particle in the classical capillary drop model wherein the interior phases are assigned bulk properties separated by interfaces of zero thickness. Surface tensions will be treated as independent of curvature but allowed composition dependence. The condensed phase chemical potentials appearing in Eq. (2.1a) are evaluated at the pressure of the vapor phase outside of the drop rather than under their own interior pressure.<sup>22</sup> The overbar serves as a reminder of this subtle distinction. Thus  $\bar{\mu}_1^{\text{sol}}$  and  $\bar{\mu}_2^{\text{sol}}$  are the chemical poten-

tials of water and salt in bulk solution having the same composition as the solution layer and  $\bar{\mu}_2^c$  is the chemical potential of bulk salt, all evaluated at the pressure of the surrounding vapor. The terms  $N\mu_1^v$  and  $n_{\text{dry}}\bar{\mu}_2^c$  cancel on evaluating free energy differences, leaving  $G_A$  in terms of contributions from the surface free energies of the two interfaces and the intervening solution:

$$G_A = G_A(n_1, n_2) = n_1(\bar{\mu}_1^{\text{sol}} - \mu_1^v) + n_2(\bar{\mu}_2^{\text{sol}} - \bar{\mu}_2^c) + \sigma_{cl}A_c + \sigma_{lv}A + C, \quad (2.1b)$$

where  $C = N\mu_1^v + n_{\text{dry}}\bar{\mu}_2^c$  depends only on temperature, external vapor pressure, and the total amounts of water and salt in the system. From the viewpoint of Eq. (2.1b), the thin layer configuration results in the limit that  $n_1$  and  $n_2$  approach zero and  $G_A$  approaches  $\sigma_{cl}A_c + \sigma_{lv}A + C \equiv G_{\text{TLC}}$ . Other authors (e.g., Ref. 9) use a dry particle predeliquescence reference state. The two approaches give equivalent results at the zero-contact-angle condition:<sup>23</sup>  $\sigma_{cv} = \sigma_{cl} + \sigma_{lv}$  (in which case  $G_{\text{TLC}} = \sigma_{cv}A_c + C$ ) where  $\sigma_{cv}$  is the dry core-vapor interfacial tension.

For fully dissolved salt ( $r_c = 0$ ) the number of salt molecules in the droplet is fixed at  $n_{\text{dry}}$  and the one equilibrium to consider is water exchange between droplet and vapor. For this case Eq. (2.1b) reduces to

$$G_B = n_1(\bar{\mu}_1^{\text{sol}} - \mu_1^v) + n_{\text{dry}}(\bar{\mu}_2^{\text{sol}} - \bar{\mu}_2^c) + \sigma_{lv}A + C. \quad (2.2)$$

## A. Equilibrium states

Consider next the partial derivatives of  $G_A$  with respect to variation of the independent composition variables  $n_1$  and  $n_2$ . From Eq. (2.1b),

$$\begin{aligned} \left(\frac{\partial G_A}{\partial n_1}\right)_{n_2} &= -\mu_1^v + \bar{\mu}_1^{\text{sol}} + \sigma_{lv}\left(\frac{\partial A}{\partial n_1}\right)_{n_2} \\ &= -\mu_1^v + \bar{\mu}_1^{\text{sol}} + \frac{2\sigma_{lv}v_1}{r}, \end{aligned} \quad (2.3)$$

where  $v_1$  is the partial molecular volume of water in solution (assumed incompressible) and  $r$  is the outer radius of the drop. (More will be said about the absence of a surface tension derivative in Sec. II B.) In carrying out such differentiations we treat  $\mu_1^v$  and  $\bar{\mu}_2^c$  as constants by fixing temperature and external vapor pressure, and use  $n_1 d\bar{\mu}_1^{\text{sol}} + n_2 d\bar{\mu}_2^{\text{sol}} = 0$  from the Gibbs–Duhem relation. (This last equality needs to be modified for small droplets to be consistent with the more complete Gibbs dividing surface model, as shown in the following section.) Terms such as  $\bar{\mu}_1^{\text{sol}}$  and  $A$  depend parametrically on the salt partitioning numbers,  $n_2$  and  $n_c = n_{\text{dry}} - n_2$ . These follow at equilibrium on setting the partial derivative with respect to  $n_2$  to zero:

$$\begin{aligned} \left(\frac{\partial G_A}{\partial n_2}\right)_{n_1} &= \bar{\mu}_2^{\text{sol}} - \mu_2^c + \sigma_{cl}\left(\frac{\partial A_c}{\partial n_2}\right)_{n_1} + \sigma_{lv}\left(\frac{\partial A}{\partial n_2}\right)_{n_1} \\ &= \bar{\mu}_2^{\text{sol}} - \mu_2^c - \frac{2\sigma_{cl}v_c}{r_c} + \frac{2\sigma_{lv}(v_2 - v_c)}{r} = 0. \end{aligned} \quad (2.4)$$

$v_2$  is the partial molecular volume of salt in solution and  $v_c$  is the volume per molecule of salt in the core. The second

equalities in Eqs. (2.3) and (2.4) use the purely geometric relations for spherical particles:

$$\left(\frac{\partial A_c}{\partial n_2}\right) = \frac{2}{r_c}\left(\frac{\partial V_c}{\partial n_2}\right) = -\frac{2}{r_c}\left(\frac{\partial V_c}{\partial n_c}\right) = -\frac{2v_c}{r_c}, \quad (2.5)$$

$$\left(\frac{\partial A}{\partial n_2}\right) = \frac{2}{r}\left(\frac{\partial V}{\partial n_2}\right) = \frac{2(v_2 - v_c)}{r}, \quad (2.6)$$

$$\left(\frac{\partial A}{\partial n_1}\right) = \frac{2}{r}\left(\frac{\partial V}{\partial n_1}\right) = \frac{2v_1}{r}. \quad (2.7)$$

$V = V_c + V_l$  is the total volume of the drop, equal to the sum of the core and solution volumes, and the salt conservation requirement,  $dn_2 = -dn_c$  is used. Differentiation of Eq. (2.2) for the fully dissolved salt droplet gives

$$\frac{dG_B}{dn_1} = -\mu_1^v + \bar{\mu}_1^{\text{sol}} + \sigma_{lv}\frac{\partial A}{\partial n_1} = -\mu_1^v + \bar{\mu}_1^{\text{sol}} + \frac{2\sigma_{lv}v_1}{r}. \quad (2.8)$$

The equilibrium chemical potential for salt in solution follows Eq. (2.4):

$$\bar{\mu}_2^{\text{sol}} = \mu_2^c + \frac{2\sigma_{cl}v_c}{r_c} - \frac{2\sigma_{lv}(v_2 - v_c)}{r}. \quad (2.9)$$

Similarly, let  $\mu_{1\text{eq}}^v$  denote the equilibrium vapor chemical potential (to distinguish from  $\mu_1^v$  which is set by the external vapor pressure) obtained by equating the right hand side of Eq. (2.3) or Eq. (2.8) to zero:

$$\mu_{1\text{eq}}^v = \bar{\mu}_1^{\text{sol}} + \frac{2\sigma_{lv}v_1}{r}. \quad (2.10)$$

This result for the fully dissolved salt droplet describes water uptake by a stable solution drop and is familiar from Köhler theory. The mixed-phase droplet, on the other hand, is in unstable equilibrium with respect to the phase partitioning of one or other of its components. This more complicated and more interesting system is investigated in the following sections.

## B. Composition and curvature dependent interfacial tension in the Gibbs dividing surface model

Equation (2.2), describing the single interface solution droplet surrounded by vapor, resembles the free energy for a binary cluster containing  $n_1$  molecules of species 1 and  $n_2 = n_{\text{dry}}$  molecules of species 2 in classical nucleation theory.<sup>18,24</sup> In that case, as here, the surface tension is assigned its bulk value, generally a function of droplet composition, and curvature effects are neglected. Progress has been made in including curvature effects in single component clusters/droplets,<sup>25</sup> but the analysis is more difficult for multicomponent systems. Fortunately, for droplets exceeding several nanometers in diameter curvature is not likely to be an important factor. For homogeneous nucleation of salt within a supersaturated droplet during efflorescence, there might well be a curvature effect due to the small (ca. 1 nanometer) diameter of the critical salt nucleus, but in the ab-

sence of quantitative information on its magnitude we will neglect curvature dependence in the present study.

In carrying out the partial differentiations, for example in Eq. (2.4), we did not include terms for the partials of  $\sigma_{lv}$  and  $\sigma_{cl}$  with respect to composition. Were the surface tension independent of composition this would be correct. The aim in this section is to show that even for the case that the surface tension is composition dependent, much of the preceding analysis applies, although to be consistent, as shown by Wilemski<sup>18</sup> in the context of classical nucleation theory, the surface excess concentrations defined in the Gibbs droplet model need to be taken into account. We show here that similar considerations apply to the deliquescence and efflorescence of small particles.

The Gibbs model resolves the occupation numbers  $n_1$  and  $n_2$  into interior and surface contributions:  $n_1 = n_{1l} + n_{1s}$ ,  $n_2 = n_{2l} + n_{2s}$ , distinguished here with subscripts  $l$  (for liquid) and  $s$ , respectively. This partitioning depends on the choice of dividing surface, which unless specified otherwise we take to be the surface of tension.<sup>26</sup> The Gibbs adsorption isotherm for the outer ( $lv$ ) interface is

$$n_{s1}d\bar{\mu}_1^{\text{sol}} + n_{s2}d\bar{\mu}_2^{\text{sol}} + Ad\sigma_{lv} = 0, \quad (2.11)$$

from which follows the composition dependence of the interfacial tension in terms of the surface excess concentrations:  $\partial\sigma_{lv}/\partial\bar{\mu}_i^{\text{sol}} = -n_{si}/A$  for species  $i$ . Interior occupation numbers enter the Gibbs–Duhem relation:

$$n_{1l}d\bar{\mu}_1^{\text{sol}} + n_{2l}d\bar{\mu}_2^{\text{sol}} = 0. \quad (2.12)$$

Similarly the interfacial tension for a small particle is evaluated at the interior composition,  $x = n_{12}/(n_{1l} + n_{2l})$ , where  $x$  is salt mole fraction in solution, and not at the total particle composition. Only in the case that  $n_{li} \approx n_i$  can Eq. (2.12) be written in terms of the total composition:  $n_1d\bar{\mu}_1^{\text{sol}} + n_2d\bar{\mu}_2^{\text{sol}} = 0$ . Otherwise, calculation of the thermodynamic properties of small particles requires explicit evaluation of the surface excess quantities in order to determine interior composition:  $n_{li} = n_i - n_{si}$ . Fortunately there is available for this purpose an independent relation between  $n_{1s}$  and  $n_{2s}$ . Following Buff<sup>27</sup> one considers the so-called “ $K$ ” dividing surface for which  $n_{s1}^K v_1 + n_{s2}^K v_2 = 0$ . This surface has the property that its separation distance from the surface of tension is related to the curvature dependence of the interfacial tension, which vanishes as the two surfaces coincide. Thus for zero curvature dependence the Buff condition,

$$n_{s1}v_1 + n_{s2}v_2 = 0, \quad (2.13)$$

applies also at the surface of tension. Equation (2.13) implies a solution volume within the surface of tension equal to the classical drop volume:

$$V - V_c = n_{1l}v_1 + n_{2l}v_2 = n_1v_1 + n_2v_2, \quad (2.14)$$

where  $V_c$  is the volume of the undissolved core for a mixed phase drop. Also equal in the two models are the surface area ( $A$ ) and drop radius ( $r$ ), whereas the droplet composition in equilibrium with vapor is given by  $\{n_{1l}, n_{2l}\}$  and not by the classical drop composition  $\{n_1, n_2\}$ . These observations are essentially those of the “revised classical theory” of Wilemski, but applied here to small particles and droplets undergo-

ing deliquescence and efflorescence. Equation (2.13) supplies an auxiliary condition that is both necessary and sufficient for Eqs. (2.2) to hold.<sup>24</sup> From another perspective, the analysis leading from Eq. (2.2) to Eq. (2.8) included neither a term in  $Ad\sigma_{lv}$  nor surface excess quantities  $n_{1s}$  and  $n_{2s}$ , but the two omissions cancel via Eqs. (2.11) and (2.12) when one begins with the more complete description of the droplet provided by the Gibbs model.

For assumed curvature independence, the addition of Eq. (2.13) provides sufficient information to compute both interior and surface occupation numbers. The interior composition follows the self-consistent, iterative solution to Eqs. (2.8) and (2.9), taking into account that  $v_1, v_2, \sigma_{lv}$ , and the solution chemical potentials are all functions of the solute mole fraction  $x = n_{12}/(n_{1l} + n_{2l})$ . The surface excess quantities are given in terms of bulk properties as follows:<sup>24</sup>

$$\begin{aligned} n_{s1} &= -A \left[ \frac{xv_2}{(1-x)v_1 + xv_2} \right] \left( \frac{d\bar{\mu}_1^{\text{sol}}}{dx} \right)^{-1} \left( \frac{d\sigma_{lv}}{dx} \right) \\ n_{s2} &= -A \left[ \frac{(1-x)v_1}{(1-x)v_1 + xv_2} \right] \left( \frac{d\bar{\mu}_2^{\text{sol}}}{dx} \right)^{-1} \left( \frac{d\sigma_{lv}}{dx} \right). \end{aligned} \quad (2.15)$$

Provided the bulk composition dependence of the surface tension and solution chemical potentials are known from models or measurement they may be inserted into these equations to obtain the surface excess quantities consistent with curvature independence.

Similar results follow for mixed phase droplets beginning with the separate application of Eq. (2.13) to each interface, but from a practical standpoint such refinement of the model is probably not worthwhile as the crystal-solution interfacial tension,  $\sigma_{cl}$ , and its dependence on composition, are largely unknown. In the absence of further information,  $\sigma_{cl}$  is treated here as constant—consistent with setting surface excess concentrations to zero.

### III. AREA CONSTRUCTIONS

The activity of salt in solution can be obtained directly from measurements of relative humidity over levitated solution droplets using an elegant graphical construction based on the Gibbs–Duhem relation.<sup>5</sup> In this bulk limit, surface tension and interior pressure effects can be neglected and the Gibbs–Duhem relation is

$$n_1d\bar{\mu}_1^{\text{sol}} + n_2d\bar{\mu}_2^{\text{sol}} = 0. \quad (3.1)$$

Using  $d\bar{\mu}_i^{\text{sol}} = kT d \ln \text{RH}$  and integrating from  $\ln \text{RH} = a$  to  $\ln \text{RH} = b$  (cf. Fig. 2), this becomes

$$\begin{aligned} \frac{\bar{\mu}_2^{\text{sol}}(a') - \bar{\mu}_2^{\text{sol}}(b'')}{kT} &= \int_a^b \left( \frac{n_1}{n_2} \right) d \ln \text{RH} \\ &\equiv A_1 + A_2 + A_6 + A_7. \end{aligned} \quad (3.2)$$

Points  $a'$  and  $b''$ , indicated in the figure, give the droplet composition at RH values corresponding to the integration limits  $a$  and  $b$ . Equation (3.2) usefully gives chemical potential differences for the nonvolatile salt in solution from measurements of the water uptake curve,  $n_1/n_2 = f_\infty(\ln \text{RH})$ , in the bulk limit of large dry particle radius and fully dissolved salt,  $n_2 = n_{\text{dry}}$ . The reduced chemical potential difference is

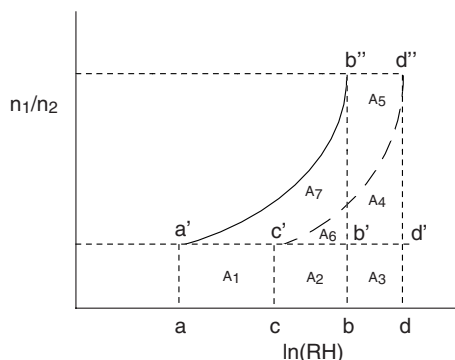


FIG. 2. Depiction of equilibrium water uptake curves for fully dissolved drops ( $n_2 = n_{\text{dry}}$ ) showing increase in drop water content as a function of increasing RH for a constant amount of salt  $n_2$ . Solid curve ( $a'b''$ ): uptake curve in the bulk limit of large  $n_2$ . Dashed curve ( $c'd''$ ): uptake curve for a small particle with  $n_2$  in the range that surface effects are important. Note shift of the equilibrium uptake curve to larger values of RH due to the Kelvin effect. Areas of various subregions ( $A_1$ – $A_7$ ) are indicate in the figure and discussed in Sec. III.

depicted in Fig. 2 by the solid curve and the relevant area is that bounded by segments  $aa'$ ,  $a'b''$ ,  $b''b$ , and  $ba$ , which is equal to the sum of regional areas specified on the right hand side of Eq. (3.2). For the case that  $a$  and  $b$  label conditions for bulk-system efflorescence and deliquescence, respectively, the area (integrating from  $a$  to  $b$ ) gives the logarithm of the salt activity at the efflorescence point relative to that of the bulk crystal in equilibrium with saturated solution of species ratio  $n_1(b'')/n_2$ , characteristic of the drop composition upon deliquescence.

### A. Free energy differences along the paths connecting initial and final droplet/mixed particle states

A similar area relation can be derived for free-energy differences. The following is a more general result that applies to small droplets as well as to the bulk limit. Substituting for  $\mu_{1\text{eq}}^v$  from Eq. (2.10) in the right hand side of Eq. (2.8) gives

$$\frac{dG_B}{dn_1} = \mu_{1\text{eq}}^v - \mu_1^v = -kT \ln\left(\frac{P_1}{P_{1\text{eq}}}\right). \quad (3.3)$$

$P_1$  is the actual water vapor pressure and  $P_{1\text{eq}}$  is the equilibrium vapor pressure over the small drop, assuming that the vapor is ideal. At vapor equilibrium  $P_1 = P_{1\text{eq}}$  and  $dG_B/dn_1 = 0$ .

A similar result follows Eqs. (2.3) and (2.4) for the mixed-phase drop. Here the path is one for which both  $n_1$  and  $n_2$  are changing, but in such a way that the salt remains in equilibrium:

$$\left(\frac{\partial G_A}{\partial n_2}\right)_{n_1} = 0. \quad (3.4)$$

Along this special path the line integral that one would normally use to evaluate changes in  $G_A$ , when  $n_1$  and  $n_2$  change arbitrarily, simplifies to integration over the  $n_1$  coordinate:

$$\left(\frac{dG_A}{dn_1}\right)_{\text{eqPath}} = \mu_{1\text{eq}}^v - \mu_1^v = -kT \ln\left(\frac{P_1}{P_{1\text{eq}}}\right). \quad (3.5)$$

Because the right hand side has the same form as in Eq. (3.3), identical expressions are obtained for free-energy differences on integration:

$$\frac{G_f - G_i}{kT} = - \int_{n_1(i)}^{n_1(f)} \ln\left(\frac{P_1}{P_{1\text{eq}}}\right) dn_1, \quad (3.6)$$

where  $i$  and  $f$  denote initial and final states under the fixed external vapor pressure  $P_1$ . Although obtained for integrations along equilibrium paths, the free-energy differences are path independent.

To illustrate application of Eq. (3.6) consider first the bulk-limit water uptake curve  $a'b''$  for the fully dissolved droplet (Fig. 2) and set  $P_1 = P_{b''}$ , so the drop having composition ratio  $n_1(b'')/n_2 = n_1(b'')/n_{\text{dry}}$  is in equilibrium. For this case the relevant area is that bounded by segments  $a'b''$ ,  $b''b'$ , and  $b'a' = A_6 + A_7$ . A small droplet having water uptake curve  $c'd''$ , and vapor pressure  $P_1 = P_{d''}$ , which is higher due to the Kelvin effect, is in equilibrium at the same composition  $n_1(d'')/n_{\text{dry}} = n_1(b'')/n_{\text{dry}}$  and the relevant area here is  $A_4 + A_6$ . Dividing both sides of Eq. (3.6) by  $n_{\text{dry}}$  we obtain for these two cases the following free-energy interpretations for the corresponding areas depicted in the figure:

$$\frac{G_{b''} - G_{a'}}{n_{\text{dry}}kT} = - \int_{a'}^{b''} \ln\left(\frac{P_b}{P_{1\text{eq}}}\right) d\left(\frac{n_1}{n_{\text{dry}}}\right) = -(A_6 + A_7), \quad (3.7)$$

$$\frac{G_{d''} - G_{c'}}{n_{\text{dry}}kT} = - \int_{c'}^{d''} \ln\left(\frac{P_d}{P_{1\text{eq}}}\right) d\left(\frac{n_1}{n_{\text{dry}}}\right) = -(A_4 + A_6),$$

with limits of integration:  $a' \equiv n_1(a')/n_{\text{dry}}$ ,  $b'' \equiv n_1(b'')/n_{\text{dry}}$ , etc. In the upper equation  $P_{1\text{eq}}$  is taken along the solid curve  $a'b''$ ; in the lower one the dashed curve  $c'd''$  is used. Notice that once  $P_{1\text{eq}}$  has somehow been determined, such integrations yield droplet free energy differences without reference to bulk properties such as surface tension, density, or even to demarcation of surface and interior properties as these are all implicit in  $P_{1\text{eq}}$ . This suggests that Eq. (3.6) is a much more general result than is implied from its present derivation based on the liquid drop/coated particle models of Sec. II. The Appendix bears this out with an alternative derivation based solely on the general kinetics of cluster evaporation and growth.

### B. Extension of the Richardson–Snyder construction to small droplets

The great utility of the Richardson–Snyder area construction [Eq. (3.2)] for direct interpretation of bulk water uptake measurements motivates its extension to small systems where surface effects play an important role. The Gibbs–Duhem relation now has to include the Laplace pressure:

$$n_{11}d\mu_1^{\text{sol}} + n_{12}d\mu_2^{\text{sol}} = VdP, \quad (3.8)$$

where  $V$  is the volume bounded by the surface of tension. Under the assumption of curvature-independent surface ten-

sion this equals the total volume of the fully dissolved salt solution as noted previously [Eq. (2.14) with  $V_c=0$ ]. The chemical potentials appearing in Eq. (3.8) (without an overbar) are defined under their own pressure, which due to the curved interface is higher inside than outside by an amount given by the Laplace relation  $\Delta P=2\sigma_{lv}/r$ . The corresponding differentials are also related:

$$\begin{aligned}d\mu_1^{\text{sol}} &= d\bar{\mu}_1^{\text{sol}} + v_1 dP \\d\mu_2^{\text{sol}} &= d\bar{\mu}_2^{\text{sol}} + v_2 dP.\end{aligned}\quad (3.9)$$

Multiplying the first and second equations by  $n_{1s}$  and  $n_{2s}$ , respectively, and adding gives

$$\begin{aligned}n_{s1}d\mu_1^{\text{sol}} + n_{s2}d\mu_2^{\text{sol}} &= n_{s1}d\bar{\mu}_1^{\text{sol}} + n_{s2}d\bar{\mu}_2^{\text{sol}} \\&\quad + (n_{s1}v_1 + n_{s2}v_2)dP \\&= n_{s1}d\bar{\mu}_1^{\text{sol}} + n_{s2}d\bar{\mu}_2^{\text{sol}} = -Ad\sigma_{lv}.\end{aligned}$$

The second equality uses the Buff relation, Eq. (2.13), and the last the Gibbs adsorption isotherm, Eq. (2.11). Adding the last result to Eq. (3.8) gives the isothermal Gibbs–Duhem relation in terms of the total occupation numbers of the solution drop:

$$n_1d\mu_1^{\text{sol}} + n_2d\mu_2^{\text{sol}} = VdP - Ad\sigma_{lv}.\quad (3.10)$$

From Eq. (3.10) we obtain a result analogous to Eq. (3.2), albeit complicated by the pressure and interfacial tension terms on the right hand side:

$$\begin{aligned}\frac{\mu_2^{\text{sol}}(c') - \mu_2^{\text{sol}}(d'')}{kT} &= \int_{c'}^{d''} \left(\frac{n_1}{n_2}\right) d \ln \text{RH} \\&\quad - \frac{1}{n_2kT} \int_{c'}^{d''} (n_1v_1 + n_2v_2)dP \\&\quad + \frac{1}{n_2kT} \int_{c'}^{d''} Ad\sigma_{lv}.\end{aligned}$$

The term in  $v_2$  accounts for the effect of increased pressure on the chemical potential of salt and can be brought to the left hand side to cancel the pressure effect in  $\mu_2^{\text{sol}}$  leaving  $\bar{\mu}_2^{\text{sol}}$ :

$$\begin{aligned}\frac{\bar{\mu}_2^{\text{sol}}(c') - \bar{\mu}_2^{\text{sol}}(d'')}{kT} &= \int_{c'}^{d''} \left(\frac{n_1}{n_2}\right) d \ln \text{RH} \\&\quad - \frac{1}{n_2kT} \int_{c'}^{d''} n_1v_1dP + \frac{1}{n_2kT} \int_{c'}^{d''} Ad\sigma_{lv} \\&= A_1 + A_2 + A_6 + A_7.\end{aligned}\quad (3.11)$$

Note that the left hand sides of Eqs. (3.11) and (3.2) are identical because for the bulk system the chemical potential is a function only of temperature and composition:  $\bar{\mu}_2^{\text{sol}}(c') = \bar{\mu}_2^{\text{sol}}(a')$  and  $\bar{\mu}_2^{\text{sol}}(d'') = \bar{\mu}_2^{\text{sol}}(b'')$ . Hence the area summations on the right hand side must also be equal. The middle integral of Eq. (3.11) requires attention. First, we use the fact that the external pressure is low (ca. 1 atm) and constant in the calculation to set  $dP=d\Delta P$  where  $\Delta P=2\sigma_{lv}/r$  is the Laplace pressure. Integrating by parts,

$$\begin{aligned}\frac{1}{n_2kT} \int_c^d n_1v_1d\Delta P &= \frac{1}{n_2kT} \left\{ [n_1v_1\Delta P]_c^d - \int_c^d \Delta P v_1 dn_1 \right\} \\&= \frac{1}{n_2kT} \left\{ [n_1v_1\Delta P]_c^d - \int_c^d \sigma_{lv}(2/r)dV \right\} \\&= \frac{n_1(d)v_1\Delta P(d)}{n_2kT} - \frac{n_1(c)v_1\Delta P(c)}{n_2kT} \\&\quad - \frac{1}{n_2kT} \int_c^d \sigma_{lv}dA,\end{aligned}$$

where compositions are evaluated along the dashed uptake curve of Fig. 2 and transformation of the integral from volume to area in the third equality uses Eq. (2.7). Substitution into Eq. (3.11) gives the final result:

$$\begin{aligned}\frac{\bar{\mu}_2^{\text{sol}}(c') - \bar{\mu}_2^{\text{sol}}(d'')}{kT} &= \int_c^d \left(\frac{n_1}{n_2}\right) d \ln \text{RH} + \frac{n_1(c)v_1\Delta P(c)}{n_2kT} \\&\quad - \frac{n_1(d)v_1\Delta P(d)}{n_2kT} \\&\quad + \frac{1}{n_2kT} \int_c^d d(A\sigma_{lv}),\end{aligned}\quad (3.12)$$

where the terms in  $Ad\sigma_{lv}$  and  $\sigma_{lv}dA$  have been combined. Each term on the right hand side has a simple area interpretation:

$$\int_c^d \left(\frac{n_1}{n_2}\right) d \ln \text{RH} = A_2 + A_3 + A_4 + A_6,\quad (3.13)$$

$$\frac{n_1(c)v_1\Delta P(c)}{n_2kT} = \frac{n_1(c)}{n_2} [\ln \text{RH}(c) - \ln \text{RH}(a)] = A_1,\quad (3.14)$$

$$\begin{aligned}\frac{n_1(d)v_1\Delta P(d)}{n_2kT} &= \frac{n_1(d)}{n_2} [\ln \text{RH}(d) - \ln \text{RH}(b)] \\&= A_3 + A_4 + A_5.\end{aligned}\quad (3.15)$$

Finally the last integral of Eq. (3.12) follows on equating the areas on the left and right hand sides of Eq. (3.12) using Eq. (3.11) for the left hand side:

$$\frac{A(d)\sigma_{lv}(d) - A(c)\sigma_{lv}(c)}{n_2kT} = A_5 + A_7.\quad (3.16)$$

This completes our extension of the Richardson–Synder area construction to small droplets. Equation (3.16) is an important result that equates the difference in dimensionless surface free energies (per molecule of salt) to the area between the bulk and small drop growth curves (Fig. 2). Approaching the bulk limit the left hand side decreases as  $1/r_{\text{dry}}$  while the right hand side also becomes smaller as the dashed curve becomes less shifted from the bulk result. Were the surface tension independent of composition, with  $Ad\sigma_{lv}=0$ , Eq. (3.16) would follow easily from the Kelvin relation for the shift in RH with reduction in drop size. The present derivation based on the Gibbs dividing surface model explicitly

takes into account the surface tension composition effect. Equation (3.16) thus provides an area construction for obtaining differences in surface free energy, which should be valid for droplets extending down to a few nanometers in diameter—beyond which curvature effects not included in the present analysis may apply.

#### IV. THIN LAYER MODEL AND DELIQUESCENCE CRITERION

##### A. General case

Consider a spherical salt particle coated with a solution layer thin enough that the total radius of the layered particle,  $r$ , can be approximated by the dry particle radius,  $r_{\text{dry}}$ , ( $r \approx r_{\text{dry}}$ ), but still thick enough to be assigned bulk thermodynamic properties in the spirit of the capillarity approximation. As the amount of salt dissolved in the thin layer is also small  $r \approx r_{\text{dry}} \approx r_c$ . These conditions describe the thin layer limit of the mixed-phase particle depicted in Fig. 1. The TLC defines a relative humidity at deliquescence ( $\text{RH}_D$ ) satisfying the simultaneous equilibrium conditions of Sec. I: (1) the chemical potential of salt in the core equals that of the dissolved salt in the thin layer and (2) the chemical potential of water in the vapor phase equals that of the water in the thin layer. These conditions are expressed more generally for solution layers of arbitrary thickness by Eqs. (2.9) and (2.10), which are now considered in the thin layer limit. Beginning with the salt equilibrium and rewriting Eq. (2.9) in reduced units with respect to  $kT$  gives

$$\begin{aligned} \frac{\bar{\mu}_2^{\text{sol}} - \bar{\mu}_2^c}{kT} &= \frac{2\sigma_{cl}v_c}{kTr_{\text{dry}}} - \frac{2\sigma_{lv}(v_2 - v_c)}{kTr_{\text{dry}}} \\ &= \frac{2((\sigma_{cl} + \sigma_{lv})v_c - \sigma_{lv}v_2)}{kTr_{\text{dry}}} \equiv \frac{2\sigma_c^{\text{eff}}v_c}{kTr_{\text{dry}}}, \end{aligned} \quad (4.1)$$

where

$$\sigma_c^{\text{eff}} = (\sigma_{cl} + \sigma_{lv}) - \sigma_{lv} \frac{v_2}{v_c} \quad (4.2)$$

is an effective surface tension that is greater (less) than  $\sigma_{cl}$  for molecular volume ratio  $v_2/v_c$  less than (greater than) unity.

Water and salt in bulk solution (chemical potentials with overbars) satisfy the constant temperature Gibbs–Duhem equation:

$$x_1 d(\bar{\mu}_1^{\text{sol}} - \bar{\mu}_1^{\text{sat}}) + x_2 d(\bar{\mu}_2^{\text{sol}} - \bar{\mu}_2^c) = 0, \quad (4.3)$$

where, following convention, we express thermodynamic properties of the bulk solution in terms of mole fractions  $x_1$  and  $x_2$  rather than the proportional molecular occupation numbers  $n_1$  and  $n_2$ .  $\bar{\mu}_1^{\text{sat}}$  is the chemical potential of water in a bulk, saturated solution of the salt. By definition  $\bar{\mu}_2^{\text{sat}} - \bar{\mu}_2^c = 0$ , determining the constant of integration for Gibbs–Duhem integration:

$$\frac{\bar{\mu}_2^{\text{sol}} - \bar{\mu}_2^c}{kT} = - \int_{\text{sat}}^{\text{sol}} \left( \frac{x_1}{x_2} \right) d \ln \text{RH} = \frac{2\sigma_c^{\text{eff}}v_c}{kTr_{\text{dry}}}. \quad (4.4)$$

The second equality presents an integral equation that can be solved numerically for the upper limit of integration,  $\ln \text{RH}_{\text{sol}}$ , as a function of  $r_{\text{dry}}$ . For this purpose one needs the water uptake curve,  $x_1/x_2$  as a function of RH for the bulk solution, and this has been measured for various salts and salt mixtures by Tang and co-workers<sup>2,4</sup> for levitated solution drops. Finally, for the deliquescence relative humidity we have from Eq. (2.10)

$$\ln \text{RH}_D = \ln \text{RH}_{\text{sol}} + \frac{2\sigma_{lv}v_1}{kTr_{\text{dry}}}. \quad (4.5)$$

Equations (4.4) and (4.5) provide a numerical route to the evaluation of  $\text{RH}_D$ . An analysis of these equations, based on a linearized expansion of the salt molality about its saturated value, and measured/estimated physicochemical properties, is being applied to recent deliquescence measurements from the Martin group at Harvard University on several different alkali-halide salts and ammonium sulfate. These results will be reported in a future publication.<sup>28</sup> Here the TLC is illustrated for the special case of an ideal solution.

##### B. Specialization to an ideal solution

For a bulk solution following Raoult's law,

$$P_w(x_2) = x_1 P_w^0 = (1 - x_2) P_w^0$$

or, equivalently,

$$\ln(\text{RH}/100) = \ln(P_w/P_w^0) = \ln x_1, \quad (4.6)$$

where  $x_1$  and  $x_2$  are the mole fractions of water and salt (modeled as nondissociating), respectfully, in the solution layer,  $P_w^0$  is the equilibrium vapor pressure over bulk liquid water and  $P_w$  is the equilibrium vapor pressure over bulk solution. Combining this last expression with Eq. (4.4) illustrates the Gibbs–Duhem integration:

$$\begin{aligned} \int_{\text{sat}}^{\text{sol}} \left( \frac{x_1}{x_2} \right)_{\text{bulk}} d \ln \text{RH} &= \int_{\text{sat}}^{\text{sol}} \frac{x_1}{x_2} d \ln x_1 \\ &= \int_{\text{sat}}^{\text{sol}} \frac{1}{x_2} dx_1 = - \int_{\text{sat}}^{\text{sol}} \frac{1}{x_2} dx_2 \\ &= - \ln \left( \frac{x_2^{\text{TLC}}}{\bar{x}_2} \right), \end{aligned} \quad (4.7)$$

where  $\bar{x}_2$  denotes the mole fraction of salt in the bulk saturated solution and the superscript “TLC” refers to the mole fraction of salt in solution satisfying the thin layer criterion. Specializing Eqs. (4.4) and (4.5) to the ideal solution gives

$$\ln \left( \frac{x_2^{\text{TLC}}}{\bar{x}_2} \right) = \frac{2\sigma_c^{\text{eff}}v_c}{kTr_{\text{dry}}} \quad (4.8)$$

and

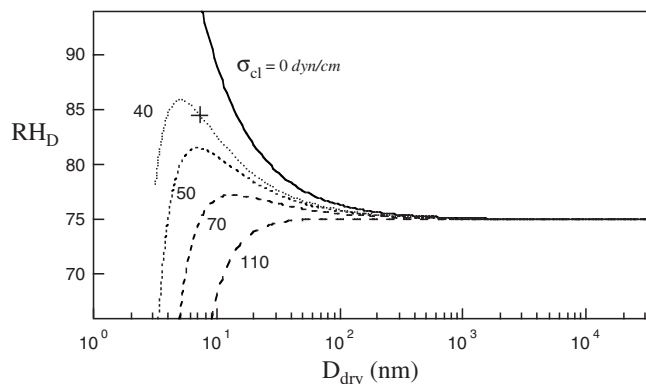


FIG. 3. Deliquescence relative humidity ( $RH_D$ ) for NaCl obtained using the thin layer criterion. Curves:  $RH_D$  as a function of dry particle diameter (nanometer) for  $\sigma_{lv}=70$  dyn/cm and the several different values of  $\sigma_{cl}$  indicated in the figure. Convergence to the bulk  $RH_D$  is seen at large dry particle size. The + sign marks the dry particle diameter of 7.2 nm and core-liquid surface tension  $\sigma_{cl}=40$  dyn/cm used throughout the calculations of Figs. 4–9.

$$\ln(RH_D/100) = \ln(1 - x_2^{\text{TLC}}) + \frac{2\sigma_{lv}v_1}{kTr_{\text{dry}}}, \quad (4.9)$$

providing a closed-form sum of Raoult's law and Kelvin terms for computing the  $RH_D$  from dry particle radius and properties of the system. Care must be taken that  $x_2^{\text{TLC}}$  remains well less than unity, a condition that Eq. (4.8) shows will be violated for very small values of  $r_{\text{dry}}$  due to failure of the ideal solution model.

## V. CALCULATIONS

Calculations are presented in the following subsections illustrating various aspects of the theory for ideal solutions.

### A. Thin layer criterion

Figure 3 shows  $RH_D$  for several different values of  $\sigma_{cl}$  as a function of dry particle diameter ( $=2r_{\text{dry}}$ ) in nanometers obtained from Eqs. (4.8) and (4.9). Curves top to bottom are for  $\sigma_{cl}=0, 40, 50, 70,$  and  $110$  dyn/cm. Thermodynamic properties, with the exception of  $\bar{x}_2$ , are from Mirabel *et al.*<sup>9</sup> for deliquescence of a generic sodium chloride crystal:  $v_1=v_2=3.03 \times 10^{-23}$  cm<sup>3</sup>,  $v_c=4.48 \times 10^{-23}$  cm<sup>3</sup>,  $\sigma_{lv}=70$  dyn/cm, and  $T=300$  K. We set  $\bar{x}_2=0.25$  to match the bulk  $RH_D$  of 75% measured by Tang *et al.*<sup>2</sup> The ideal solution curves of Fig. 3 show  $RH_D$  passing through a maximum, which shifts to larger dry diameter and becomes less distinct with increasing product  $\sigma_c^{\text{eff}}v_c$  achieved here by increasing  $\sigma_{cl}$  [Eq. (4.2)]. For sufficiently large  $\sigma_c^{\text{eff}}v_c$  the indication is a uniform decrease in  $RH_D$  with decreasing dry diameter due to dominance of Raoult's law leading term in Eq. (4.9). Such behavior is not seen in the NaCl measurements but a different salt, KI, does show the decrease in  $RH_D$  with decreasing dry particle size for particle diameters smaller than about 60 nm, the upper range of the measurements.<sup>28</sup> For larger particles the TLC curves are seen to approach the bulk  $RH_D$  value independent of the core-liquid surface tension.

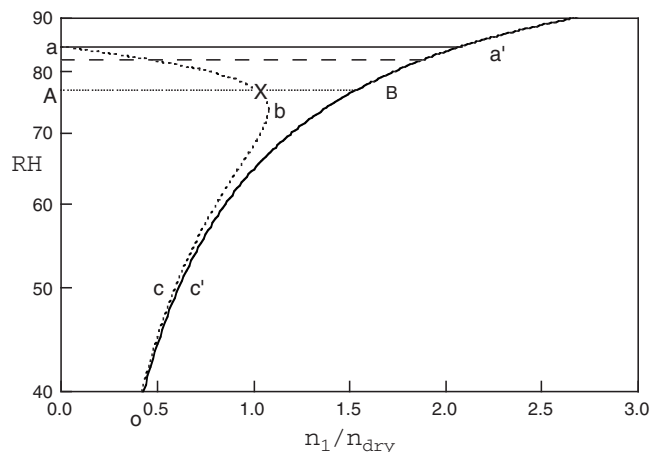


FIG. 4. Phase diagram for particle-droplet transformation of NaCl-water droplets showing RH (logarithmic scale) vs  $n_1/n_{\text{dry}}$ . Dotted curve: equilibrium states of the mixed-phase particle beginning with thinly coated salt (a) and following increasing dissolution of the salt core through states (X), (b), (c), and finally (o), the state of complete dissolution for which  $r_c=0$ . Solid curve: equilibrium states of the fully dissolved solution droplet showing uptake of increasing amounts of water with increasing RH through conditions (o), (c'), (B), and (a'). Line  $a-a'$  marks the activationless deliquescence transition at the  $RH_D$  (84.5%). The dashed horizontal line marks a nucleated deliquescence transition just below the  $RH_D$ . Line  $A-X-B$  marks the equal area construction for free energy equality. Points  $c'$  and  $c$  mark approximate location of the initial and critical efflorescence states, respectively.

### B. Phase diagram

Figure 4 shows the relative humidity in equilibrium with the layered particle over the full range of layer thickness (dotted curve) for dry particle diameter of 7.2 nm and  $\sigma_{cl}=40$  dyn/cm. The deliquescence relative humidity,  $RH_D=84.5\%$ , is from Eqs. (4.8) and (4.9). These conditions are marked by the + sign of Fig. 3 and the intercept point “a” of Fig. 4. Phase diagrams were also computed for several different conditions along the various curves of Fig. 3 by the methods to be described but since the results are similar to those presented here, we limit discussion to this particular case. General points along the dotted curve of Fig. 4 are obtained numerically from Eqs. (2.3) and (2.4) (the thick layer model) on equating salt and water activities between the crystal-solution and solution-vapor phases, respectively. The solid curve shows the relative humidity in equilibrium with the single-phase solution drop following Eqs. (2.9) and (2.10). The solid horizontal line ( $a-a'$ ) is located at the  $RH_D$ . The dashed horizontal line marks a nucleated deliquescence transition just below the  $RH_D$ . Nucleation rates under these conditions are largely a function of nucleation barrier height (Fig. 5). The horizontal line ( $A-X-B$ ), at  $RH=77.0\%$ , gives conditions at free-energy equality  $G_A=G_B$ , with  $G_A$  from Eq. (2.1b) in the limit that  $n_1$  and  $n_2$  approach zero, and  $G_B$  from Eq. (2.2) for the fully dissolved solution drop, both calculations carried out at this same value of RH. This example shows the free-energy equality criterion underestimating  $RH_D$  by more than 7%. Similar phase diagrams, in different coordinates, were obtained by Shchekin *et al.*,<sup>29</sup> in their recent thermodynamic study of droplet formation around a soluble condensation nucleus.

Figure 4 illustrates the phase rule for macroscopically

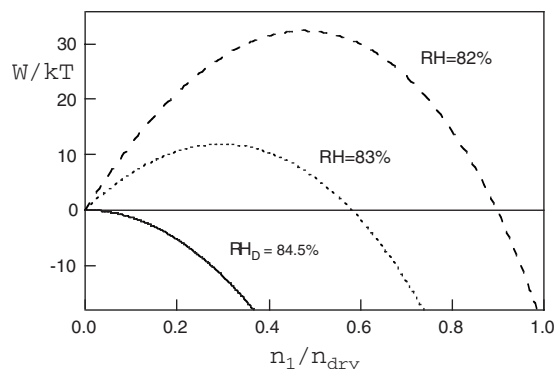


FIG. 5. Reversible work of mixed-phase NaCl-water particle formation relative to the thin layer reference state. Figure shows the presence of a nucleation barrier at relative humidities below the  $RH_D$ . Deliquescence occurs without barrier at the  $RH_D$  and by barrier crossing at lower RH values (e.g., the middle and upper curves).

small systems under different pressures from curved interfaces. This rule takes the form  $f=c+1$ , independent of the number of phases, where  $f$  is the number of degrees of freedom and  $c$  (here equal to 2) is the number of components.<sup>30,31</sup> Thus with temperature and dry particle size fixed, the sole remaining degree of freedom is RH along each of the mixed-phase and single-phase branches shown in the figure. Positive slope regions, the lower portion ( $ocb$ ) of the mixed-phase branch and the entire single-phase branch, are in stable equilibrium with respect to the exchange of water. The upper portion ( $ab$ ) of the mixed-phase branch is in unstable equilibrium with respect to water, but stable with respect to exchange of salt between the solution and undissolved core. The lower portion is in unstable equilibrium with respect to the exchange of salt. These stability properties become clear on inspection of the free-energy surfaces (Figs. 8 and 9).

### C. Applications of the area construction: Nucleation barrier and free-energy surfaces

The following analysis requires the reversible work of forming mixed-phase particles and single-phase solution drops starting from the thin layer configuration. This is the free-energy difference:

$$W(n_1, n_2) = G(n_1, n_2) - G_{\text{TLC}}, \quad (5.1)$$

where  $G_{\text{TLC}}$ , the free-energy of the thin layer configuration, follows Eq. (2.1b) in the limit that  $n_1$  and  $n_2$  approach zero. For notational simplicity the dependence on dry particle size  $n_{\text{dry}}$  and relative humidity have been omitted from Eq. (5.1). For  $n_2 = n_{\text{dry}}$  we have the case of fully dissolved core and  $G(n_1, n_2) = G_B(n_1, n_2)$  [Eq. (2.2) and solid curve of Fig. 4]. Along the mixed-phase branch, which is the dotted curve of Fig. 4,  $G = G_A$ . In the thin layer limit both  $n_1$  and  $n_2$  are small compared to  $n_{\text{dry}}$ , which conditions are marked by point “a” along the dotted curve. On replacing water vapor pressure with relative humidity, the general result of Eq. (3.6) becomes

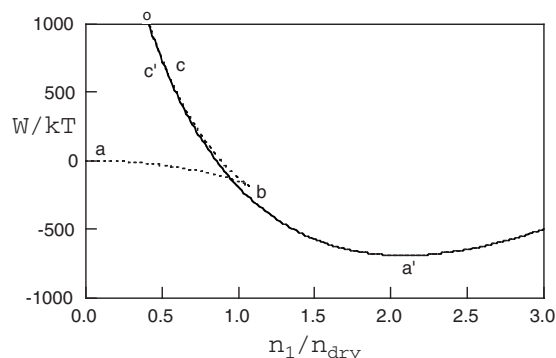


FIG. 6. Free energy of NaCl-water particle formation at deliquescence. Reversible work for forming the mixed-phase particle (dashed curve  $a-b-c-o$ ) and the solution drop (solid curve  $o-c'-a'$ ). RH is fixed at the  $RH_D$  and free energy is taken relative to the thin layer limit ( $a$ ). State labels follow Fig. 4. The figure shows substantial lowering of free energy (by about  $700kT$ ) accompanying deliquescence at the  $RH_D$ . States ( $a$ ) and ( $a'$ ) exhibit maximum and minimum values in free energy corresponding to unstable and stable equilibrium, respectively, with respect to water vapor exchange.

$$\frac{W_{\text{RH}}(n_1, n_2)}{kT} = -n_{\text{dry}} \int_0^{n_1/n_{\text{dry}}} \ln\left(\frac{\text{RH}}{\text{RH}_{\text{eq}}}\right) d\left(\frac{n_1'}{n_{\text{dry}}}\right), \quad (5.2)$$

with limits of integration from the initial thin layer configuration  $n_1'(i) \approx 0$  to the final state  $n_1'(f) = n_1$  where  $n_1'$  is a dummy integration variable. The subscript on  $W$  indicates that the integral is evaluated for a prescribed constant value of RH while  $\text{RH}_{\text{eq}}$ , which is a function of  $n_1'/n_{\text{dry}}$ , follows the phase diagram curves of Fig. 4. The integration path follows the curve ( $a-X-b-c-o$ ) for the mixed-phase branch and continues ( $o-c'-B-a'$ ) along the single-phase branch, noting the change in sign for  $dn_1'$ , first at the location “b” of the maximum in  $n_1'/n_{\text{dry}}$  along the mixed-phase branch, and again at  $o$ . Inspection of Eq. (5.2) and Fig. 4 reveals a geometric interpretation for  $W$  in terms of areas bounded by the various curves and lines shown in the figure. The condition of free-energy equality is given by the Maxwell-like equal area construction, line ( $A-X-B$ ), with the area bounded by line segment  $A-X$  and the upper portion of the mixed-phase branch, curve ( $a-X$ ), equal to the area of the lower crescent, bounded by curves ( $X-b-c-o$ ), ( $o-c'-B$ ), and line segment ( $X-B$ ). The free-energy difference at the  $RH_D$  ( $G_{\text{TLC}} - G_B$  at  $\text{RH} = 84.5\%$ ) is substantial. In Fig. 4 this difference is shown geometrically as proportional to the large crescent-shaped area bounded by curves ( $a-X-b-c-o$ ), ( $o-c'-B-a'$ ), and line ( $a-a'$ ). This illustrates (see also Fig. 6) the large reduction in free-energy accompanying (irreversible) deliquescence at the  $RH_D$ .

Nucleation barriers to deliquescence for fixed values of the relative humidity, at and slightly below the  $RH_D$  (for example at the RH indicated by the dashed horizontal line of Fig. 4), are shown in Fig. 5. For given RH the barrier maximum is located at the crossing point of the corresponding horizontal line and the top portion of the mixed phase branch (Fig. 4). The barrier height is proportional to the area bounded by this line segment and the mixed-phase curve up to the crossing point. It is seen that both the barrier height and the critical layer thickness vanish at the  $RH_D$ . But slightly below the  $RH_D$  deliquescence can be seen as a nucle-

ation process requiring fluctuations to surmount the barrier. Depending on kinetics, such fluctuations are likely to be effective only for barrier heights less than about  $10kT$ – $15kT$ , implying that for this dry particle diameter (7.2 nm), and larger, the nucleation of deliquescence cannot occur at RH values much below the  $RH_D$ , as there the barrier heights would be too large to have an appreciable crossing rate. Figure 5 shows barrier profiles for three different RH values and the fixed dry particle size. In general, the smaller the dry particle size, which enters through the prefactor  $n_{dry}$  in Eq. (5.2), the smaller the barrier and the wider the range of RH over which nucleation can occur. In the dry particle size range of available measurements (particles with diameter greater than about 5 nm) the nucleation effect is essentially not observable given the typical 1%–2% uncertainty in measurement of RH. On the other hand, for particles with diameters approaching 1–2 nm, it should be possible to see deliquescence significantly below the  $RH_D$ . Although size is the main factor controlling crossing rate, other variables including observation time and material properties, for different salts, also need to be taken into account. A more complete analysis of the kinetics of deliquescence barrier crossing is underway and will be presented in future publications.

The full range of integration of Eq. (5.2), with RH held constant at the  $RH_D$ , is shown in Fig. 6. This is the activationless (no-barrier) case and the early portion of the trace from  $a$  to  $b$  matches the solid curve of Fig. 5. The sign changes in  $dn_1$  at  $b$  and  $o$  are evident as cusps in the figure. Deliquescence to the stable drop at  $a'$  is seen to occur with a sizeable decrease in free energy with  $G_{TLC}$  exceeding  $G_B$  by about  $700kT$ , in clear violation of the free energy equality criterion. The presence of the barrier (Fig. 5), which for all practical purposes is crossable only near the  $RH_D$ , prevents the transition from occurring at lower RH where the initial and final state free energies are equal. Integration of Eq. (5.2) with RH held constant at 50% is shown in Fig. 7 (other quantities have the same values as in Fig. 6). These conditions are representative of those at the efflorescence nucleation transition ( $c' \rightarrow c$ ). Both  $c'$  and  $c$  are stable minima with respect to exchange of water. Point  $c$  describes a small salt particle in (unstable) equilibrium with highly supersaturated salt solution. This is the critical nucleus configuration for efflorescence and it is seen to be slightly higher in free energy than the pre-efflorescent drop at  $c'$ . The difference is in fact equal to the barrier height for nucleation of salt from the supersaturated drop. The reference thin layer state is off scale at the origin of the figure.

#### D. Transformation of free-energy surfaces and extensions of the nucleation theorem

To excellent approximation, properties inherent to the particle/drop specified by  $n_1$  and  $n_2$ , which include surface tension, density, and evaporation rate, are all independent of the external vapor RH. Indeed this is the key assumption behind the general derivation of Eq. (3.6) given in the Appendix. As a result, the free-energy surfaces for different values of RH are simply related. To see this, choose some

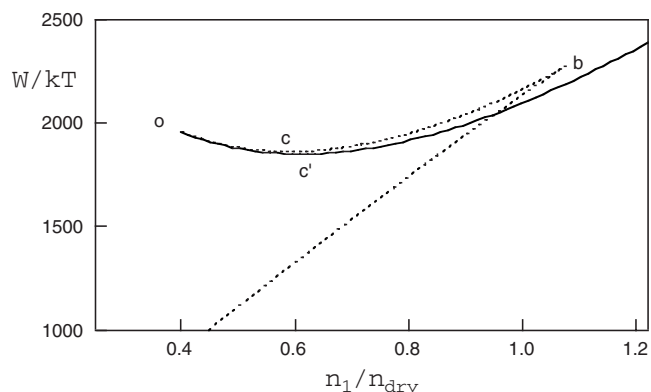


FIG. 7. Free energy of NaCl-water particle formation near efflorescence. Reversible work relative to the thin-layer limit for forming the mixed-phase particle (dashed curve  $o$ - $c$ - $b$ - $a$  where state “ $a$ ” is off scale at the origin) and the solution drop (solid curve  $o$ - $c'$ ) at  $RH=50\%$ , which is near the measured efflorescence nucleation transition. State labels follow Fig. 4.  $c'$ - $c$  is the efflorescence transition. This is slightly uphill in energy (by about  $14kT$ , which is the free energy needed to form the critical salt nucleus under these conditions) and is accompanied by some loss of water from the particle. Both  $c$  and  $c'$  represent stable equilibria with respect to exchange of water. The mixed particle state  $c$  (consisting of the critical nucleus in solution) is unstable both to dissolution (return to  $c'$ ) and core growth, with much lower energy achievable by core growth.

convenient reference relative humidity, for example the  $RH_D$ . Evaluating Eq. (5.2) at the  $RH_D$  and subtracting gives an especially transparent result:

$$W_{RH}(n_1, n_2) = W_{DRH}(n_1, n_2) - n_1 kT \ln \left( \frac{RH}{RH_D} \right), \quad (5.3)$$

where  $W_{DRH}(n_1, n_2)$  is the free-energy surface for external relative humidity fixed at the  $RH_D$  and the effect of any change in RH lies in the second term on the right. Equation (5.3) completes the unification of deliquescence and efflorescence processes by showing connection between constant RH cross sections of the three-dimensional free-energy surface  $W_{RH}(n_1, n_2)$ . Including those cross sections for RH values near deliquescence and efflorescence. A similar situation occurs classically with the free-energy barriers describing nucleation from ideal vapors.

Figures 8 and 9 show the corresponding binary free-energy surfaces,  $W_{DRH}(n_1, n_2)$  and  $W_{ERH}(n_1, n_2)$ , respectively, from Eqs. (2.1) and (2.2). Superimposed on the contours are the mixed-phase particle and fully dissolved ( $n_2/n_{dry}=1$ ) branches from the phase diagram of Fig. 4. These are identical curves in each figure. Contours crossing the mixed-phase branch have vertical slopes according to Eq. (3.4) as is evident in the figure. This is true even near the binary saddle point marking the critical nucleus for efflorescence in Fig. 9, although the limited contour line resolution here makes this difficult to see. Contour levels are not marked in the figures but can be inferred in the case of Fig. 9 by locating crossings with the single- and mixed-phase branches and using Fig. 7 to interpolate the corresponding free energies.

Differentiation of Eq. (5.3) yields an important step toward derivation of a nucleation theorem applicable to deliquescence and efflorescence processes:

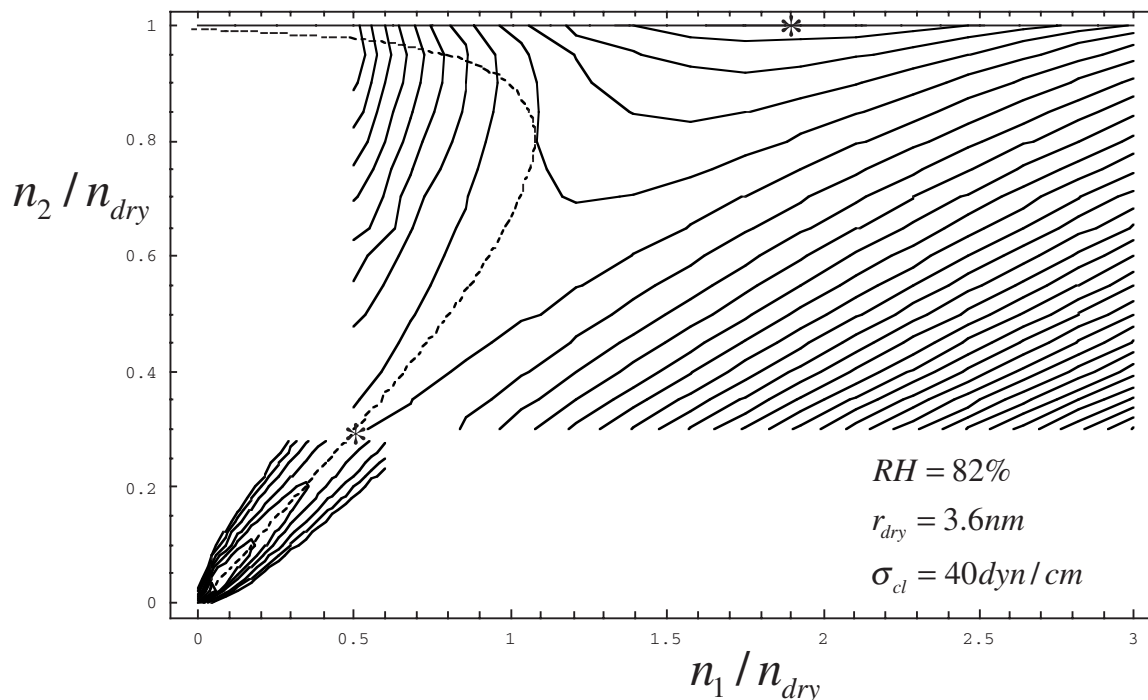


FIG. 8. Free-energy surface at relative humidity slightly below the  $RH_D$ . The lower portion of the figure shows the nucleation barrier and the asterisk marks the critical nucleus. The dotted curve and horizontal line mark the mixed-phase and fully dissolved solution branches from the phase diagram of Fig. 4. The upper asterisk marks the deliquescence final state.

$$\frac{1}{kT} \left[ \frac{\partial W(n_1, n_2)}{\partial \ln RH} \right]_{T, n_1, n_2} = -n_1. \quad (5.4)$$

Equation (5.4) applies to clusters of any size and is in essence a consequence of the law of mass action invoked with

the ideal vapor assumption made in the derivation of Eq. (5.2) (Appendix). In order to relate this derivative to the rate of nucleation, and hence to experiment, the derivative must be obtained at the saddle point of the barrier  $W^* = W(n_1^*, n_2^*)$ , which corresponds to the critical cluster size.

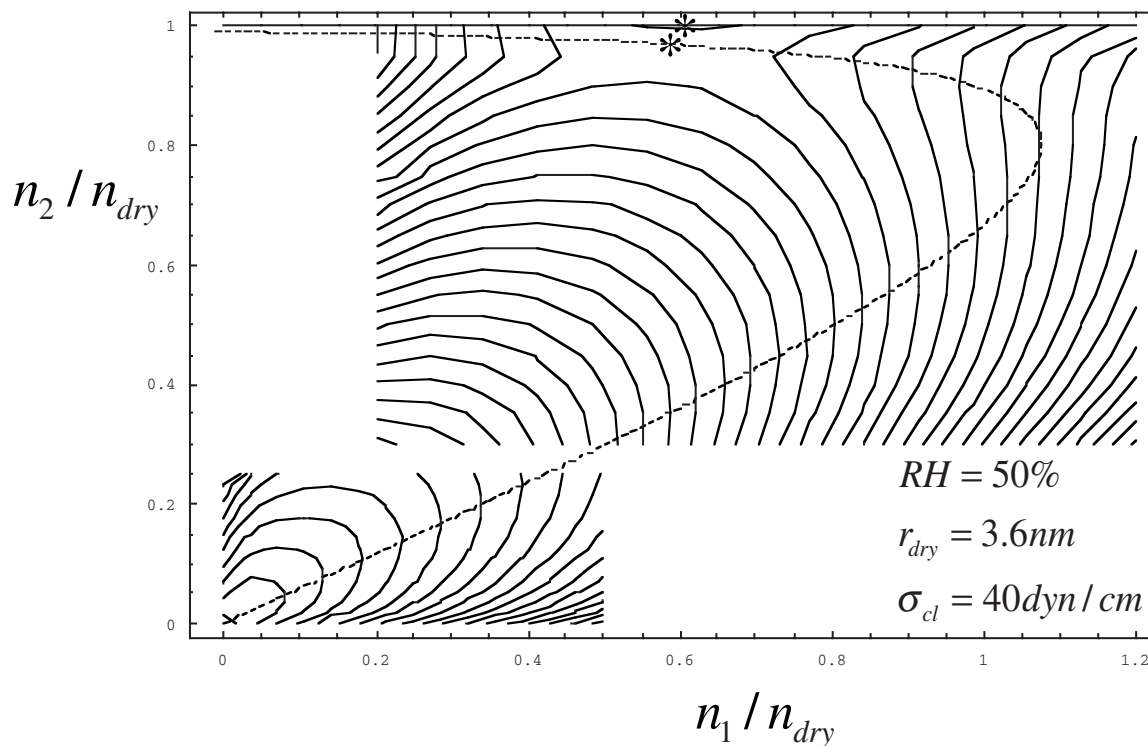


FIG. 9. Free-energy surface at relative humidity near efflorescence. The upper portion of the figure shows the binary nucleation surface and the lower asterisk here marks the critical salt nucleus in unstable equilibrium with the surrounding solution drop. The dotted curve and horizontal line mark the mixed-phase and fully dissolved solution branches from the phase diagram of Fig. 4. The upper asterisk marks the initial metastable solution droplet just prior to efflorescence. Upon barrier crossing the system undergoes irreversible lowering of free energy arriving at the origin of the figure (a thinly coated salt particle and surrounding vapor).

Since, in particular,  $n_1^*$  is itself a function of RH, we use the fact that  $(\partial W/\partial n_1)_{n_1^*}=0$ , which is the case both at the initial and critical states for efflorescence (states  $c$  and  $c'$  of Fig. 7) and at the deliquescence barrier maximum [see Eq. 10 of Ref. 32].

For deliquescence the initial thin layer configuration has  $W=0$  and  $n_1^*$  is the number of water molecules in the critical solution layer. Thus the barrier height for the process is  $\Delta W_{\text{del}}^*=W(n_1^*)$ . Using Eq. (5.4) and maximum condition gives the nucleation theorem for deliquescence:

$$\frac{1}{kT} \left( \frac{\partial \Delta W_{\text{del}}^*}{\partial \ln \text{RH}} \right)_T = -n_1^*. \quad (5.5)$$

Here a decrease in barrier height follows an increase in RH in accordance with Fig. 5. Note that Eq. (5.5) follows immediately from the area interpretation of the barrier height, given above in connection with Fig. 4, and the fundamental theorem of calculus. For efflorescence the barrier height takes the form  $\Delta W_{\text{eff}}^*=W(c)-W(c')$  to give just a slightly more complicated extension of the nucleation theorem:

$$\frac{1}{kT} \left( \frac{\partial \Delta W_{\text{eff}}^*}{\partial \ln \text{RH}} \right)_T = n_1(c') - n_1(c). \quad (5.6)$$

Here, because the number of water molecules in the particle is higher for state  $c'$  than it is for  $c$  (cf. Fig. 7), Eq. (5.6) yields a decrease in barrier height with decrease in RH in agreement with observations. Locations  $c$  and  $n_1^*$  are binary saddle points of  $W$  marked by asterisks in Figs. 8 and 9. Note that both saddle points lie on the mixed-phase branch of the phase diagram, another common feature of the two processes, while the initial state for efflorescence (location  $c'$  of Fig. 7) and the final state for deliquescence lie on the solution branch, and are also indicated by asterisks in the two figures.

In addition to a loss of water upon efflorescence, Fig. 9 shows that a significant fraction (several percent) of the total salt in the small drop is used to form the (even smaller) salt critical nucleus within that drop. Unlike efflorescence from bulk solution, which is usually described as a single component nucleation process, these small systems require a fully binary treatment in order to take into account limited material availability and changes in composition of both components.

## VI. SUMMARY AND DISCUSSION

It is useful to summarize similarities between deliquescence and first-order phase transformation. We have seen how single-particle free-energy equality,  $G_A=G_B$ , can be interpreted geometrically using a Maxwell-like equal area construction (Fig. 4), but that this condition does not describe the deliquescence transition except in the bulk limit. For smaller particles the transition occurs instead either in the metastable regime, by a nucleation process, or at the threshold for instability where the nucleation barrier itself vanishes and the process becomes activationless. The latter condition, analogous to entering a spinodal regime, is determined by the thin layer criterion.

The thin layer criterion predicts onset of deliquescence under the condition of simultaneous equilibrium between salt in the undissolved particle core and in the thin solution layer, and between water in the thin layer and the surrounding vapor. For RH values below the TLC there is already a strong driving free energy that would otherwise force the process sooner were it not for the nucleation barrier, which first vanishes precisely at the point that the TLC holds. From this viewpoint the deliquescence transformation is kinetically limited (by the barrier) rather than thermodynamically controlled. Nevertheless, this kinetics is largely hidden for dry particle radii greater than just a few nanometers where deliquescence can only be observed at the instability threshold, much like with the Köhler-theoretic activationless transformation of cloud condensation nuclei into droplets, which occurs at the joining of the stable and unstable branches of the phase diagram governing water-particle exchange.<sup>15</sup> For deliquescence, at any given undersaturation ( $\text{RH}_D-\text{RH}$ ) the nucleation barrier quickly exceeds many  $kT$  with increase in dry particle size and even very small changes in RH lead to large (many  $kT$ ) changes in barrier height in accord with the nucleation theorem [Eq. (5.5)]. This circumstance presents a barrier that has in effect has either vanished or is insurmountable—just as in Köhler theory. The present theory predicts that for dry particle radii approaching 1–2 nm there be a measurable range of RH values, below the  $\text{RH}_D$  of the thin layer criterion, for which one has the intermediate case: surmountable barrier heights of just a few  $kT$  and crossing rates determined by nucleation theory (in detail this will depend on material properties and observation time as well as on particle size).

The present theory exhibits strong similarities between deliquescence and efflorescence that are not evident in the bulk. These include common area constructions for the free energy changes associated with these processes and a common free-energy surface. Setting RH in Eq. (5.3) equal to the efflorescence relative humidity  $\text{RH}_E$  shows the only difference (at constant temperature) between the free energy surfaces of Figs. 6 or 8, for deliquescence, and Figs. 7 or 9, for efflorescence, is term proportional to  $n_1$ :

$$W_{\text{ERH}}(n_1, n_2) = W_{\text{DRH}}(n_1, n_2) + n_1 kT \ln \left( \frac{\text{RH}_D}{\text{RH}_E} \right). \quad (6.1)$$

Accordingly, information on efflorescence is contained within the deliquescence free-energy surface and vice versa. For example, a point along the ridge of maxima at constant  $n_1$ , seen along the upper branch of the mixed-phase curve (dashed curve of Fig. 8 near  $n_1/n_{\text{dry}}=0.58$ ), becomes on lowering of the relative humidity to the ERH the saddle point for nucleation of efflorescence indicated by the asterisk in Fig. 9. Such similarities only become apparent when the efflorescence is treated, as it is here, as a fully binary nucleation process. This unified view opens the door for powerful methods developed historically within the context of nucleation theory to be carried over to the deliquescence and efflorescence of small particles. The methods developed in this paper included: (1) application of kinetic potential theory, (2)

applications of nucleation concepts such as capillarity, self-consistent nucleation theory, and the Gibbs dividing surface, (3) extension of nucleation theorems to relate change in deliquescence and efflorescence barrier heights to changes in RH and difference in number of water molecules (positive or negative) in the particle/drop, and (4) demonstration that the binary free energy surfaces for deliquescence and efflorescence are linear in  $\ln$  RH (in the presence of ideal vapor) and related through Eq. (6.1).

## ACKNOWLEDGMENTS

This research was supported by the DOE Atmospheric Sciences Program. The authors thank DOE GCEP fellow Mackenzie Smith, Dr. Amanda Mifflin, Dr. George Biskos, and Professor Scot Martin of Harvard University for sharing results from their measurements prior to publication. Discussions with Dr. Susan Oatis during the early stages of this work are greatly appreciated.

## APPENDIX: MICROSCOPIC DERIVATION OF EQS. (3.6) and (5.2)

In this appendix an alternative derivation of the reversible work [left hand side of Eq. (5.1)] is presented using detailed balance considerations applied to the kinetics of particle evaporation and growth. The approach is conceptually more straightforward than the thermodynamic derivation used to obtain Eqs. (3.6) and (3.7) and suggests a generality for these equations that extends well beyond the capillary drop models of Sec. II. What follows closely parallels the kinetic potential formulation of nucleation theory.<sup>19</sup>

Consider the exchange of water vapor between particles of size  $g$  and  $g+1$  where  $g$  now replaces  $n_1$  as the number of water molecules in the particle. The total number of salt molecules present independent of phase remains fixed at  $n_{\text{dry}}$ . According to detailed balance,

$$\beta_g n_g = \gamma_{g+1} n_{g+1}, \quad (\text{A1})$$

where  $\beta_g(\gamma_g)$  is the rate of water vapor condensation onto (evaporation from) a particle of size  $g$ . The constrained equilibrium concentration of clusters,  $n_g$ , satisfies the Boltzmann relation:

$$n_g \propto \exp\left(-\frac{W(g)}{kT}\right), \quad (\text{A2})$$

where  $W(g)$  is the reversible work required to form a particle of size  $g$ . From Eqs. (A1) and (A2),

$$\frac{W(g+1) - W(g)}{kT} = \ln\left(\frac{n_g}{n_{g+1}}\right) = \ln\left(\frac{\gamma_{g+1}}{\beta_g}\right). \quad (\text{A3})$$

Adding such differences for a sequence of evaporation/condensation steps gives

$$\begin{aligned} \frac{W(g_2) - W(g_1)}{kT} &= \ln\left(\frac{n_{g_1}}{n_{g_2}}\right) \\ &= \ln\left(\frac{n_{g_1} n_{g_1+1} \dots n_{g_2-1}}{n_{g_1+1} n_{g_1+2} \dots n_{g_2}}\right) \\ &= -\ln\left(\frac{\beta_{g_1} \beta_{g_1+1} \dots \beta_{g_2-1}}{\gamma_{g_1+1} \gamma_{g_1+2} \dots \gamma_{g_2}}\right) \\ &= -\sum_{g=g_1}^{g_2-1} \ln\left(\frac{\beta_g}{\gamma_{g+1}}\right). \end{aligned} \quad (\text{A4})$$

The right hand side of Eq. (A4) has been called the kinetic potential.<sup>19</sup> This is an expression solely in terms of rate constants, which is here equal to the difference in the reduced thermodynamic potentials  $W/kT$  of particles of sizes  $g_2$  and  $g_1$ .

For a single particle in equilibrium with its vapor the condensation rate  $\beta_g^{\text{eq}}$  equals the evaporation rate  $\gamma_{g+1}$ . This allows Eq. (A4) to be rewritten using the identity

$$\frac{\beta_g}{\gamma_{g+1}} = \frac{\beta_g \beta_g^{\text{eq}}}{\beta_g^{\text{eq}} \gamma_{g+1}} = \frac{\beta_g}{\beta_g^{\text{eq}}}, \quad (\text{A5})$$

in the form

$$\frac{W(g_2) - W(g_1)}{kT} = -\sum_{g=g_1}^{g_2-1} \ln\left(\frac{\beta_g}{\beta_g^{\text{eq}}}\right) = -\sum_{g=g_1}^{g_2-1} \ln\left(\frac{P_1}{P_{1\text{eq}}(g)}\right). \quad (\text{A6})$$

The last equality makes use of the proportionality between vapor condensation rate and vapor pressure for ideal vapors. Any accommodation coefficient different from unity will affect both sides of Eq. (A1) equally and cancel from the final result.  $P_1$  is the actual vapor pressure and  $P_{1\text{eq}}(g)$  is that pressure of vapor for which the particle of size  $g$  is in equilibrium with its environment. Note that the critical size  $g = g^*$ , for which  $P_{1\text{eq}}(g^*) = P_1$ , maximizes  $W(g)$  and makes no contribution to the cumulative sum in Eq. (A6), as expected at an extremum in  $W$ . Converting the right hand side from summation to integration yields the more general, molecular-based, derivation of Eq. (3.6) (and Eq. (5.2)) we seek:

$$W(g_2) - W(g_1) = -kT \int_{g_1}^{g_2} \ln\left(\frac{P_1}{P_{1\text{eq}}(g)}\right) dg \quad (\text{A7})$$

In computer simulations of cluster dynamics it has been found expedient to first obtain the evaporation rate and then use detailed balance to get the condensation rate. Thus the right hand side of Eq. (A4) can, in principle, be evaluated by combining computer simulation- or theory-based estimates of the cluster evaporation rate with detailed balance. One possible computational approach is to use variational transition state methods similar to those that have been employed in dynamical nucleation theory in order to estimate size-dependent molecular-cluster evaporation rates.<sup>33</sup>

<sup>1</sup>S. T. Martin, *Chem. Rev. (Washington, D.C.)* **100**, 3403 (2000).

<sup>2</sup>I. N. Tang, H. R. Munkelwitz, and N. Wang, *J. Colloid Interface Sci.* **114**, 409 (1986).

<sup>3</sup>C. B. Richardson and T. D. Snyder, *Langmuir* **10**, 2462 (1994).

- <sup>4</sup>I. N. Tang and H. R. Munkelwitz, *J. Geophys. Res.* **99**, 18801 (1994).
- <sup>5</sup>K. Hameri, M. Vakeva, H.-C. Hansson, and A. Laaksonen, *J. Geophys. Res.* **105**, 22231 (2000).
- <sup>6</sup>K. Hameri, A. Laaksonen, M. Vakeva, and T. Suni, *J. Geophys. Res.* **106**, 20749 (2001).
- <sup>7</sup>G. Biskos, A. Malinowski, L. M. Russell, P. R. Buseck, and S. T. Martin, *Aerosol Sci. Technol.* **40**, 97 (2006).
- <sup>8</sup>G. Biskos, L. M. Russell, P. R. Buseck, and S. T. Martin, *Geophys. Res. Lett.* **33**, L07801 (2006).
- <sup>9</sup>P. Mirabel, H. Reiss, and R. K. Bowles, *J. Chem. Phys.* **113**, 8200 (2000).
- <sup>10</sup>Y. S. Djikaev, R. Bowles, H. Reiss, K. Hameri, A. Laaksonen, and M. Vakeva, *J. Phys. Chem. B* **105**, 7708 (2001).
- <sup>11</sup>L. M. Russell and Y. Ming, *J. Chem. Phys.* **116**, 311 (2002).
- <sup>12</sup>T. B. Onasch, R. McGraw, and D. Imre, *J. Phys. Chem. A* **104**, 10797 (2000).
- <sup>13</sup>Y. Gao, S. B. Chen, and L. E. Yu, *Atmos. Environ.* **41**, 2019 (2007).
- <sup>14</sup>I. N. Tang and H. R. Munkelwitz, *Atmos. Environ.* **27A**, 467 (1993).
- <sup>15</sup>P. Mirabel, H. Reiss, and R. K. Bowles, *J. Chem. Phys.* **113**, 8194 (2000).
- <sup>16</sup>Y. S. Djikaev, *J. Chem. Phys.* **116**, 9865 (2002).
- <sup>17</sup>Q. Dai, J. Hu, and M. Salmeron, *J. Phys. Chem. B* **101**, 1994 (1997).
- <sup>18</sup>G. Wilemski, *J. Chem. Phys.* **80**, 1370 (1984).
- <sup>19</sup>D. T. Wu, *Solid State Phys.* **50**, 37 (1997).
- <sup>20</sup>D. Kashchiev, *J. Chem. Phys.* **76**, 5098 (1982).
- <sup>21</sup>R. McGraw and D. Wu, *J. Chem. Phys.* **118**, 9337 (2003).
- <sup>22</sup>H. Reiss, *Methods of Thermodynamics* (Dover, Mineola, 1996), Chap. 11.
- <sup>23</sup>P. G. de Gennes, *Rev. Mod. Phys.* **57**, 827 (1985).
- <sup>24</sup>A. Laaksonen, R. McGraw, and H. Vehkamäki, *J. Chem. Phys.* **111**, 2019 (1999).
- <sup>25</sup>R. McGraw and A. Laaksonen, *J. Chem. Phys.* **106**, 5284 (1997).
- <sup>26</sup>S. Ono and S. Kondo, in *Encyclopedia of Physics*, edited by S. Flugge (Springer, Berlin, 1960), Vol. 10, p. 134.
- <sup>27</sup>F. Buff, *Z. Elektrochem.* **56**, 311 (1952).
- <sup>28</sup>E. R. Lewis, R. McGraw, S. T. Martin, M. Smith, G. Biskos, A. L. Mifflin (in preparation).
- <sup>29</sup>A. K. Shchekin, I. V. Shabaev, and A. I. Rusanov, *J. Chem. Phys.* **129**, 214111 (2008).
- <sup>30</sup>A. Firoozabadi, *Thermodynamics of Hydrocarbon Reservoirs* (McGraw-Hill Professional, New York, 1999), p. 114.
- <sup>31</sup>M. E. Wise, S. T. Martin, L. M. Russell, and P. R. Buseck, *Aerosol Sci. Technol.* **42**, 281 (2008).
- <sup>32</sup>R. K. Bowles, R. McGraw, P. Schaaf, B. Senger, J.-C. Voegel, and H. Reiss, *J. Chem. Phys.* **113**, 4524 (2000).
- <sup>33</sup>S. M. Kathmann, G. K. Schenter, and B. C. Garrett, *J. Chem. Phys.* **111**, 4688 (1999).